Acadlore Transactions on Geosciences
https://www.acadlore.com/journals/ATG

Dynamic Responses of Embankment Dams, Constituted from Varied Soil Types, to Seismic Activity

Mohammad Shouib Anwar Khan, Mohsen Seyedi*

Departmen of Civil Engineering, School of Engineering and Architecture, Altinbas University, 34217 Istanbul, Turkey

* Correspondence: Mohsen Seyedi (mohsen.seyedi@altinbas.edu.tr)

Received: 08-01-2023 **Revised:** 09-03-2023 **Accepted:** 09-08-2023

Citation: M. S. A. Khan and M. Seyedi, "Dynamic responses of embankment dams, constituted from varied soil types, to seismic activity," *Acadlore Trans. Geosci.*, vol. 2, no. 3, pp. 177–187, 2023. https://doi.org/10.56578/atg020305.

Abstract: This research delineates a numerical elucidation concerning the flow through an embankment, utilising PLAXIS2D software, and underscores the pivotal influence of soil composition—encompassing gravel, sand, and clay—on the structural resilience of embankments during seismic events. Different material models, incorporating the UBC3D-PLM for sand and the Hardening Soil (HS) small constitutive models for gravel and clay, were strategically employed to replicate embankment behaviours, ensuring a meticulous simulation of distinct soil types. The objective herein was to scrutinise the impact of dynamic loads and soil typologies on pertinent variables: settlements, lateral displacements, and excess pore water pressure engendered within the embankment. A comprehensive series of 2D finite element models, each representative of a specific soil type, were formulated and subsequently subjected to an earthquake record for dynamic analysis. It was discerned that embankments constituted from sand and gravel exhibited a pronounced settlement under dynamic loads, relative to those formulated from clay, primarily attributable to the absence of cohesion forces, augmented porosity, and diminished energy dissipation efficacy. Such factors render sand and gravel more prone to compression and settlement upon exposure to dynamic loads. Moreover, embankments fabricated from sand were identified to generate superior pore pressures compared to their clay or gravel counterparts, a phenomenon attributable to sand's compressibility which can engender augmented volumetric strains and initiate pumping phenomena, thereby elevating pore pressures. In contrast, gravel and clay materials demonstrated enhanced drainage capabilities and reduced compressibility, facilitating the proficient dissipation of excess pore pressures.

Keywords: Finite element method; Embankment; PLAXIS2D; Settlement; Excess pore pressure

1 Introduction

Embankment dams, ubiquitously recognised as earth fill dams, embody structures typically composed of soil and rock, where the impermeable core serves to inhibit water seepage whilst permeable layers facilitate its drainage. From diminutive irrigation barriers to substantial water storage infrastructures, embankment dams, characterised by meticulous construction under strict engineering protocols, meticulously account for dam height, materials, and site conditions [1]. Ongoing surveillance and maintenance are imperatively necessitated to assure their sustainable functionality in flood control and hydroelectric power generation.

In the realm of embankment dam construction, a pivotal influence is exerted by soil type on variables such as displacement, settlements, and pore water pressure generation. Cohesive soils, such as clay, utilised for impermeable cores, have been observed to mitigate displacement and sliding, given that compaction is executed proficiently to curtail settlements. Conversely, factors such as the soil's porosity and permeability have been discerned to profoundly influence pore water generation. Consequently, achieving optimal seepage control and pore pressure mitigation necessitates the meticulous design of cores, alongside efficacious filter and drainage layers. Additionally, elements inclusive of toe design, slope grading, and material arrangement coalesce to enhance embankment dam safety and stability, necessitating scrupulous soil selection and engineering to forestall structural failures, unequal settlements, and seepage predicaments, which could potentially compromise safety.

Seepage and excess pore pressure generation within embankment dams, which have the potential to undermine their stability, potentially leading to breaches, must be astutely mitigated [2]. An escalation in pore water pressure within the dam compromises its stability and can precipitate internal erosion and piping, a process wherein soil particles are eroded away, instigating the creation of voids and channels within the dam [3, 4]. Left unaddressed, such voids can progressively enlarge, diminishing the dam's water-holding capacity and, ultimately, culminating in catastrophic dam failure, unleashing torrents of water downstream, thereby engendering flooding and infrastructural damage in proximate regions.

In the context of embankment dams, geometric design emerges as a significant determinant, influencing seepage and pore pressure generation. A myriad of factors, encompassing dam height, slope, crest width, core thickness, presence of filter and drainage zones, spillway and outlet design, foundation and abutment characteristics, and hydraulic structures, jointly exert a pronounced influence on seepage and pore pressure regulation [5]. Therefore, an assiduous examination of these design parameters is imperative to minimise the likelihood of internal erosion, piping, and additional failures, thereby assuring the long-term stability of the dam whilst proficiently regulating seepage and pore pressure.

In recent decades, a multitude of experimental and numerical studies have embarked on investigations into the stability and deformations of embankment dams under seismic conditions [6–8]. Examinations into the generation of excess pore water pressure inside dams and liquefaction of the embankment soil have also been conducted [9–12]. Furthermore, diverse methodologies aiming to preclude liquefaction [13–15], erosion [16], seepage [17], and instability [18] within embankment soil have been proposed and studied across various literature. However, an in-depth parametric investigation assessing the performance of various soil types in embankment dam construction, especially under seismic conditions, warrants further exploration and discussion.

The pivotal role of soil types in embankment dam construction, and their substantial impact on engineering aspects such as settlement, lateral movement, and pore pressure accumulation during seismic events, have been rigorously investigated in the present study. Involving the formulation of three distinct embankment dam models utilising sand, gravel, and clay, and leveraging the finite element program PLAXIS2D, the models were subjected to an earthquake record, post which, dynamic responses encompassing lateral displacements, vertical settlements, and pore pressure generations were calculated and comprehensively compared.

2 Methodology

In geotechnical engineering analyses, PLAXIS2D, denoted henceforth as a versatile finite element analysis programme, affords substantial utility for modelling a spectrum of geotechnical challenges [19]. Esteemed for its capability to facilitate meticulous soil-structure interaction analyses, adapt customisable material models, navigate complex geometries and loadings, it is additionally accredited for its competencies in safety assessment, visualisation tools application, parametric studies, documentation, and provision of a user-friendly interface. This tool, serving as an instrumental resource, allows engineers to scrutinise the stability and performance of embankment dams under various conditions, encapsulating the simulation of real-world scenarios through meticulous modelling of material behaviour, boundary condition definition, and execution of advanced analyses.

The simulation of embankment dams via PLAXIS 2D systematically transpires in two integral steps. Initially, the construction of the embankment model is executed, succeeded by the induction of a static steady-state analysis, whereby the stability of the model in a drained condition is verified. Subsequently, dynamic analysis is employed, subjecting the model to seismic loading by applying an earthquake acceleration record at the model's base, thereby emulating the dynamic response of the embankment soil under undrained conditions.

Undrained conditions are notably conducive to the generation of pore water pressure within the soil. During the static analysis phase, lateral boundaries of the model were established to sustain an equal degree of freedom (equal DOF) condition. In contrast, throughout the dynamic analysis phase, free-field boundaries, representative of drained material, were utilized to emulate the distant field, adhering to recommendations delineated in the PLAXIS2D manual. The base of the model was constrained in both horizontal and vertical dimensions, whilst lateral boundaries were constrained solely in the horizontal aspect.

For the modelling of the embankment dams, two constitutive soil models were implemented: The HS model, instrumental in modelling gravel and clay, and the UBC3D-PLM (where PLM denotes PLAXIS Liquefaction Model), pivotal for the modelling of sand. Embankment dam numerical modelling necessitates the incorporation of innovative and nuanced constitutive models to precisely epitomise material behaviour, enhance predictive capability, and amplify safety and risk assessment. These models empower engineers to simulate intricate material responses, optimize dam designs, evaluate long-term performance whilst adhering to regulatory standards, and mitigate environmental impacts. Such models facilitate the depiction of non-linear and time-dependent behaviours, providing data-driven decision-making tools to enhance the reliability and efficiency of embankment dams throughout their operational lifespan.

The geometric delineation and the strategic measurement points of the numerical model are illustrated in Figure 1, while the earthquake acceleration record, as applied to the embankment dam model base, is portrayed in Figure 2.

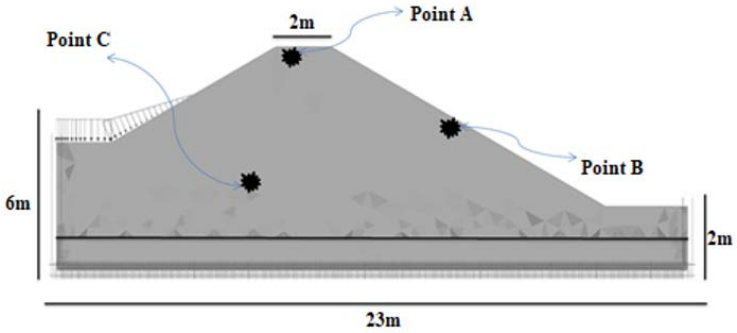

Figure 1. Geometric representation and measurement points of the embankment

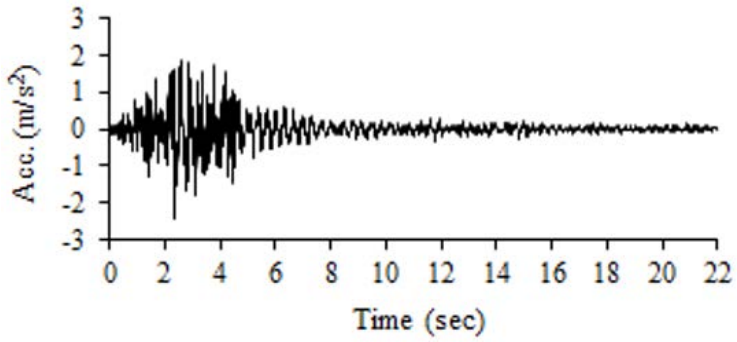

Figure 2. Earthquake acceleration record implemented in the model

The HS Small model, elucidated in the study [20], is characterised as an isotropic hardening elasto-plastic model, incorporating two pivotal yield surfaces: a shear hardening yield surface, akin to the hyperbolic law, and capable of expansion towards the Mohr-Coulomb failure criterion, contingent on deviatoric plastic strain, and a Cap yield surface, which, governed by plastic volumetric strains, demarcates the compressive stress path elastic region. In a contrasting vein, the UBC3D-PLM model exemplifies an effective stress elasto-plastic model, exhibiting capabilities to simulate the liquefaction behaviour of sands under seismic loading [21].

Presented in Table 1 are the input parameters deployed for modelling gravel and clay utilising the HS Small model. Notably, a Poisson atio v and reference pressure $\mathrm{P_{ref}}$ were uniformly considered to be 0.25 and 100kPa, respectively, across all soil models in the study.

Table 1. Experimental parameters

Soil	$\mathbf{D_r}$	$\gamma_{\mathbf{sat}}$ $(\mathbf{kN/m^3})$	$\mathbf{E_{50}}^{\mathbf{ref}}$ $(\mathbf{kN/m^2})$	$\mathbf{E_{oed}}^{\mathbf{ref}}$ $(\mathbf{kN/m^2})$	$\mathbf{E_{ur}}^{\mathbf{ref}}$ $(\mathbf{kN/m^2})$	$\mathbf{G_0}^{\mathbf{ref}}$ $(\mathbf{kN/m^2})$	$\mathbf{m}$	$\gamma_{0.7}$	φ' (°)	$\mathbf{C'_{ref}}$ $(\mathbf{kN/m^2})$
Clay	50	19.4	30000	30000	90000	94000	0.54	1.5×10^{-4}	34	20
Gravel	80	19.8	48000	48000	144000	114000	0.45	1.2×10^{-4}	38	0

Input parameters, as rendered in Table 1, were determined by employing Eqs. (1) to (8).

$$\gamma_{\mathrm{sat}} = 19 + 1.6\frac{D_r}{100} \tag{1}$$

$$E_{\mathrm{oed}}^{\mathrm{ref}} = E_{50}^{\mathrm{ref}} = 60000\frac{D_r}{100} \tag{2}$$

$$\mathrm{E_{ur}^{ref}} = 180000\frac{\mathrm{D_r}}{100} \tag{3}$$

$$G_0^{ref} = 60000 + 68000\frac{D_r}{100} \tag{4}$$

$$m = 0.7 - \frac{D_r}{320} \tag{5}$$

$$\gamma_{0.7} = \left(2 - \frac{D_r}{100}\right) \times 10^{-4} \tag{6}$$

$$\varphi' = 28 + 12.5\frac{D_r}{100} \tag{7}$$

$$R_f = 1 - \frac{D_r}{800} \tag{8}$$

Table 2 elucidates the input parameters utilised in modelling sand via the UBC3D-PLM model.

Table 2. Input parameters employed in the UBC3D-PLM soil model

Soil	$\mathbf{D_r}$	γ_{sat} $(\mathbf{kN/m^3})$	$(N_1)_{60}$	$\mathbf{K_{G^*e}}$	$\mathbf{K_{B^*e}}$	$\mathbf{K_{G^*p}}$	$\mathbf{m_e}$	$\mathbf{n_e}$	$\mathbf{n_p}$	φ_{CV} (°)	$\mathbf{R_f}$
Sand	50	20	11	964	675	450	0.5	0.5	0.4	33	0.77

Eqs. (9) to (13) served as the computational means to ascertain the input parameters delineated in Table 2.

$$(N_1)_{60} \approx \frac{(D_r)^2}{15^2} \tag{9}$$

$$K_G^{*e} = 21.7 \times 20 \times (N_1)_{60}^{0.333} \tag{10}$$

$$K_B^{*e} = 0.7 \times K_G^{*e} \tag{11}$$

$$K_G^{*p} = 0.003 \times K_G^{*e} \times (N_1)_{60}^2 + 100 \tag{12}$$

$$R_f \approx 1.1 \times (N_1)_{60}^{-0.15} < 0.99 \tag{13}$$

3 Results

3.1 Displacement Analyses of Embankment Dams

Following the execution of dynamic analyses on three disparate embankment dam models, a calculated portrayal of results, encapsulating vertical and lateral displacements in conjunction with excess pore pressure, was formulated and graphically depicted. Figure 3 and Figure 4 facilitate a comparative exploration of vertical settlements and lateral displacements across different soil matrices at designated points A and B, respectively. It is delineated from the visual representations that embankment dams, when constructed from clay, manifest markedly pronounced lateral and vertical movements when juxtaposed with those comprised of gravel and sand under seismic loadings.

Crucially, the elevated propensity of clay embankment dams to experience such displacement can be ascribed to several engineering properties inherent to clay. Principally, the lower shear strength typically exhibited by clay relative to both gravel and sand escalates its susceptibility to shear deformation amidst seismic occurrences. Moreover, the pronounced plasticity characteristic of clay facilitates deformation without concurrent fracturing, precipitating substantial lateral deformations as the material undergoes plastic deformation under the lateral forces imparted by seismic activity. Furthermore, the notable sensitivity of clay to variations in water content, which can induce a softening effect and thereby augment susceptibility to deformation and consolidation amidst an earthquake, is also a contributory factor.

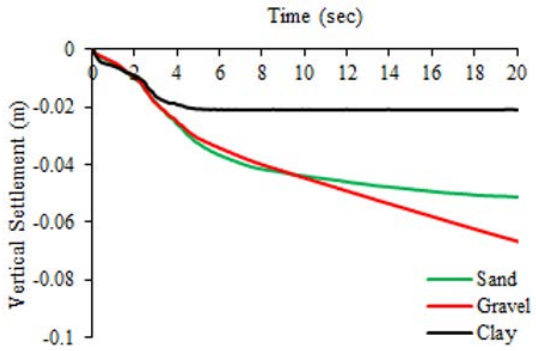

Figure 3. Comparative analysis of vertical displacements, calculated at point A, across varied embankment models

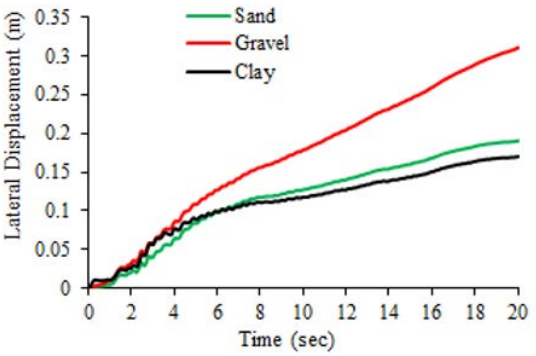

Figure 4. Comparative assessment of lateral displacements, evaluated at point B, across distinct embankment models

3.2 Examination of Excess Pore Pressure

Figure 5 juxtaposes the excess pore pressure results secured at point C (referenced in Figure 1), illustrating a heightened generation of excess pore pressure in sandy soil under earthquake loading when contrasted with clay or gravel. This phenomenon may be attributed to the distinct permeability and compressibility inherent to sand. The typically elevated permeability of sand, relative to gravel and clay, permits water to traverse more freely through interstitial voids between particles, catalysing a more rapid accumulation of excess pore pressure. Additionally, the compressibility of sand surpasses that of gravel yet remains inferior to clay. Owing to the impact of soil particle compressibility on water expulsion from the soil matrix, the generation of excess pore pressure is markedly evident in sand relative to both gravel and clay.

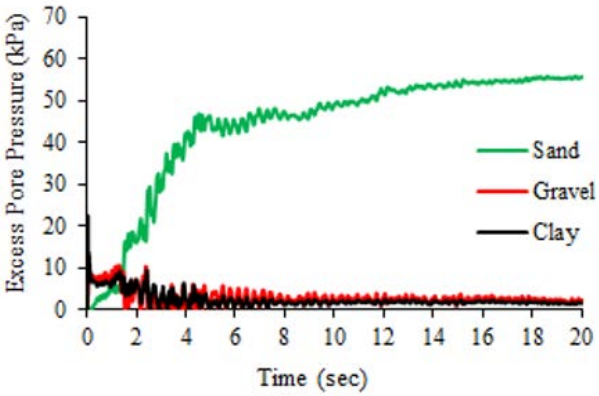

Figure 5. Comparative exploration of excess pore pressure, calculated at point C, across different embankment models

3.3 Graphical Illustrations of Displacement Results

Figure 6, Figure 7, Figure 8, Figure 9, Figure 10, Figure 11 illustrate graphical representations of displacement results, derived from numerical analyses, with the highest displacements observed to transpire in the crest and face of the embankment dams.

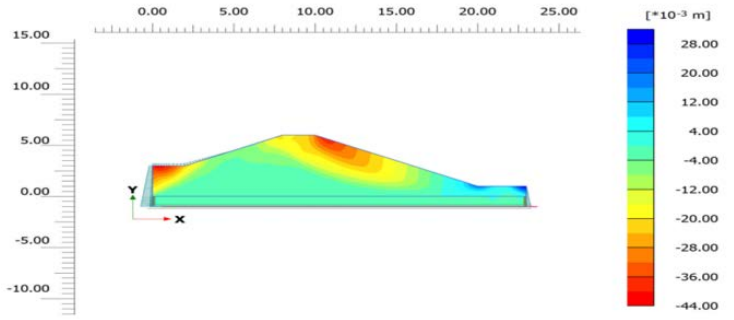

Figure 6. Vertical displacement U_y observed in an embankment constructed from clay, subjected to seismic loading

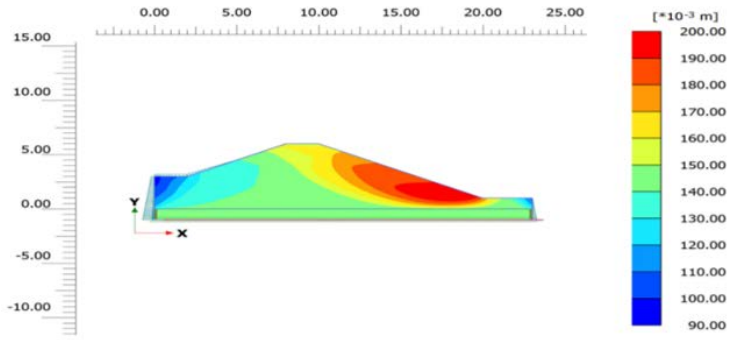

Figure 7. Lateral displacement U_x noted in an embankment constructed from clay, under the influence of seismic loading

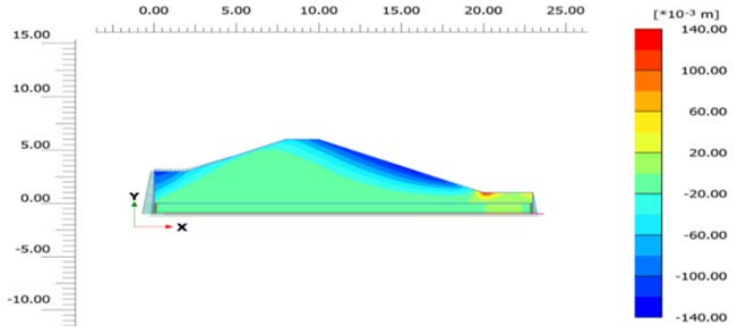

Figure 8. Vertical displacement U_y in an embankment constructed from gravel, subjected to seismic loading

3.4 Active Pore Pressure Analysis

Figure 12, Figure 13, Figure 14 furnish graphical visualisations of active pore pressure results procured from numerical analyses, revealing the maximal active pore pressure to occur in proximity to the bedrock of the embankment dams, attributable to the closeness of bottom layers to the earthquake record, the vibrational source.

3.5 Correlation with Existing Literature

Notably, analogous studies in extant literature have affirmed the efficacy and capability of employing PLAXIS 2D in modelling the dynamic responses of embankment dams subjected to ground motions [22, 23].

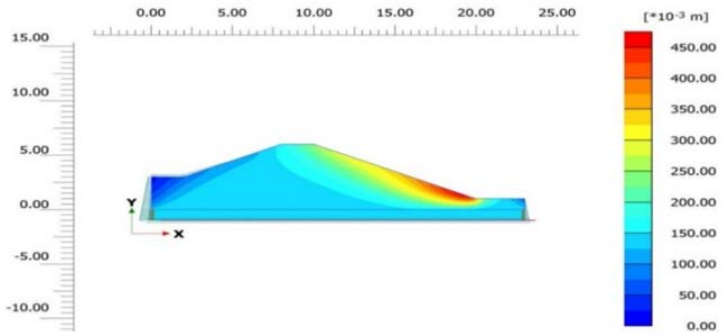

Figure 9. Lateral displacement U_x recorded in an embankment constructed from gravel, under seismic loading conditions

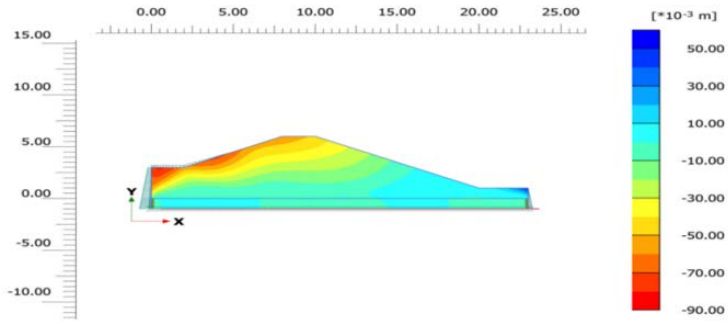

Figure 10. Vertical displacement U_y observed in an embankment constructed from sand, subjected to seismic loading

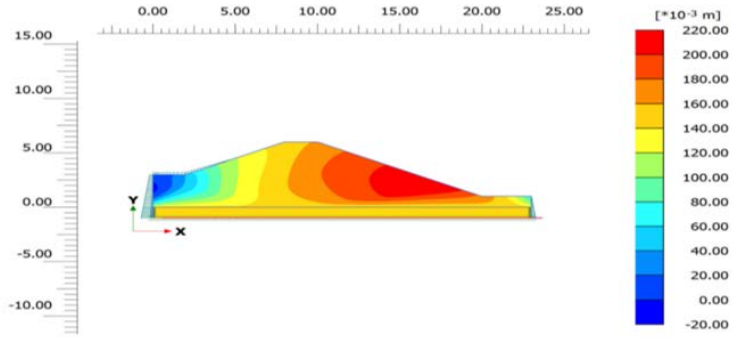

Figure 11. Lateral displacement U_x noted in an embankment constructed from sand, during seismic loading

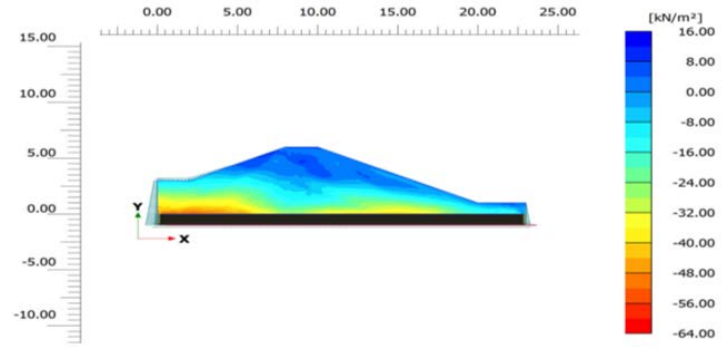

Figure 12. Active pore pressure p_{active} in an embankment constructed from clay

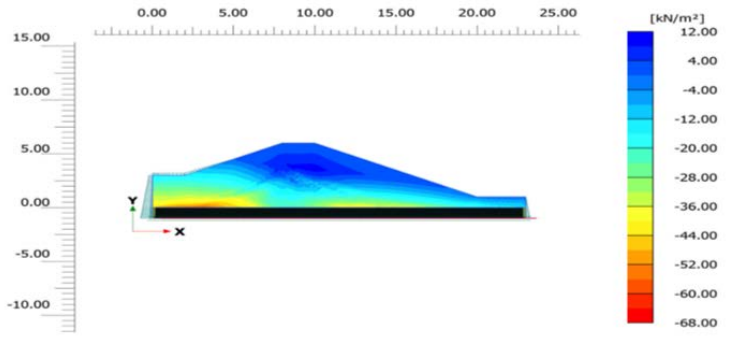

Figure 13. Active pore pressure p_{active} in an embankment constructed from gravel

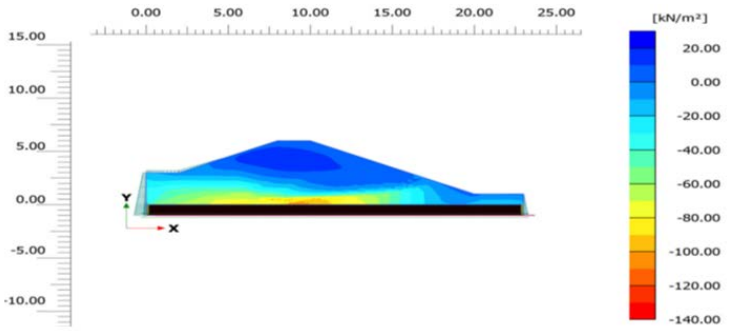

Figure 14. Active pore pressure p_{active} in an embankment constructed from sand

4 Discussion

The nuanced distinctions among distinct soil matrices, evident through the numerous graphical representations and analyses delineated in previous sections, provoke contemplation regarding the aptitude of various soil types in embankment dam construction, especially amidst seismic activities.

Displacement disparities across the varied soil types, illuminated in section 3.1, convey pronounced behavioural dissimilarities in the context of seismic loadings. The prominent lateral and vertical movements within clay-based embankments, relative to their gravel and sand-based counterparts, suggest that clay, while manifesting a considerable degree of plasticity and reduced shear strength, tends to succumb to deformations under the exertions of seismic forces. The rationale behind this could be illuminated by exploring more deeply the mechanical behaviours and stress-strain relationships intrinsic to clay in a dynamic setting.

In a parallel vein, the discernment of elevated excess pore pressure generation in sand, as depicted in Figure 5 and expounded upon in section 3.2, invites further exploration into the hydraulic conductivity and drainage characteristics inherent to sandy soils. The amplification of pore pressure in sandy soils during seismic activity, an aspect attributable to its enhanced permeability and particular compressibility, renders this soil type a focal point for future investigations into the correlation between granular structure, interstitial water movement, and induced pressures under dynamic loadings. It provokes an enquiry: does the degree of compressibility and the size of interstitial voids influence the rapidity and magnitude of pore pressure accumulation amidst seismic activity?

The insights derived from displacement analyses, particularly the visualisations proffered by Figure 6, Figure 7, Figure 8, Figure 9, Figure 10, Figure 11, necessitate a closer examination into the geometrical and mechanical stability of embankment dams. The observations of maximal displacements within the crest and face regions of the embankments under seismic loading introduce the prospect of evaluating structural redesigns and reinforcements aimed at ameliorating these vulnerabilities. This could mean an exploration into alternative construction methodologies, materials, or incorporation of seismic mitigation technologies such as base isolators or energy dissipators.

A scrutiny of active pore pressure variations, depicted through Figure 12, Figure 13, Figure 14, reveals a penchant for maximal pressures to materialise in proximity to the bedrock of the embankment dams. This indication of a relationship between proximity to vibrational sources and active pore pressure generation imparts an avenue for investigation into the potential of designing countermeasures which mitigate these pressure accruals, such as implementing pressure-relieving systems or utilising materials with enhanced dilative properties at strategic locations.

The thematic alignment of the results procured in this study with prior literature, particularly the corroborative nature of these findings in relation to prior research employing PLAXIS 2D for embankment dam dynamic response

modelling [22, 23], underscores the reliability and replicability of such methodological approaches. Yet, it also portends the exigency for future research to penetrate deeper into the realms of practical application, exploring, for instance, how these numerical models and findings translate into real-world scenarios, and how engineers might utilise this data in enhancing the seismic resilience of embankment dams in various geographical and geological contexts.

In synthesis, while the insights gleaned from these analyses fortify the understanding of embankment dam behaviours under seismic influences, they concurrently unveil a plethora of avenues warranting further exploration, encapsulating the domains of material science, structural engineering, geotechnical modelling, and seismic risk mitigation, all towards the pivotal end of fortifying civil infrastructures against the latent perils of seismic activities.

5 Conclusions

The present study elucidates the impact of varied soil engineering properties on the structural integrity of embankment dams, employing a finite element program to simulate dynamic responses. Differing embankments, constructed from distinct soil types—namely sand, clay, and gravel—were scrutinized, with an acceleration time history being applied at the model's base. From the dynamic analyses, essential data regarding vertical and lateral displacements, in addition to excess pore pressures, were procured at various measurement points.

A discernible distinction in displacement behaviours was observed amongst fine- and coarse-grained soils. Fine-grained soil, exemplified by clay, exhibited diminished displacements, attributable to its low permeability and elevated plasticity. In contrast, coarse-grained soils, such as gravel and sand, demonstrated augmented displacements, likely due to their heightened permeability and suboptimal interlocking characteristics. Moreover, given that the compressibility and permeability of sand surpass those of clay and gravel, the imposition of cyclic loading on embankments formed from sand culminated in an escalated generation of excess pore pressure, thereby amplifying the liquefaction potential under severe ground motions.

The findings herein serve as a pivotal guide, enabling geotechnical engineers to safeguard dams and adjacent communities. A comprehensive understanding of seismic vulnerabilities, derived from these outcomes, facilitates the application of apt improvement techniques, thereby mitigating potential failures and instabilities in embankment dams induced by seismic activity.

It is imperative to note that although the findings provide insightful data regarding the seismic behaviours of embankment dams constructed from varied soil types, further investigative endeavours may focus on exploring a more extensive range of soil types and seismic conditions. In future studies, the incorporation of diverse seismic loading conditions and additional soil mechanical properties may yield more exhaustive insights into the stability of embankment dams under varied seismic influences. Furthermore, an exploration into the comparative long-term behaviours of embankments under static and dynamic loads could provide additional practical insights for engineering applications.

Data Availability

The data used to support the findings of this study are available form the corrsponding author upon request.

Conflicts of Interest

The authors declare that they have no conflicts of interest.

References

[1] A. D. M. Penman, "On the embankment dam," *Géotechnique*, vol. 36, no. 3, pp. 303–348, 1986. https://doi.org/10.1680/geot.1986.36.3.303

[2] D. C. Froehlich, "Embankment dam breach parameters and their uncertainties," *J. Hydraul. Eng.*, vol. 134, no. 12, pp. 1708–1721, 2008. https://doi.org/10.1061/(asce)0733-9429(2008)134:12(1708)

[3] S. Johansson, "Seepage monitoring in embankment dams," Doctoral Disseration, University of Belgrade, Serbia, 1997.

[4] C. F. Wan and R. Fell, "Investigation of rate of erosion of soils in embankment dams," *J. Geotech. Geoenviron.*, vol. 130, no. 4, pp. 373–380, 2004. https://doi.org/10.1061/(asce)1090-0241(2004)130:4(373)

[5] V. I. B. D. Mello, "Practice, precedents, principles, problems, and prudence in embankment dam engineering," in *Symposium Problem Practice of Dam Engineering, Bangkok*, 1980, pp. 3–17. https://victorfbdemello.com.br/arquivos/Publicacoes/084.1%20-%20PRACTICE%20,%20PRECEDENTS,%20PRINCIPLES,%20PROBLEMAS,%20AND%20PRUDENCE.pdf

[6] J. R. Swaisgood, "Embankment dam deformations caused by earthquakes," in *Pacific Conference on Earthquake Engineering*, 2003. http://nzhttp://nzsee.org.nz/db/2003/View/Paper014s.pdfsee.org.nz/db/2003/View/Paper014s.pdf

[7] G. Hunter and R. Fell, "The deformation behaviour of embankment dams," 2003. https://vm.cihttps://vm.civeng.unsw.edu.au/uniciv/R-416.pdfveng.unsw.edu.au/uniciv/R-416.pdf

[8] M. Seid-Karbasi and P. M. Byrne, "Embankment dams and earthquakes," *Int. J. Hydropow. Dams*, vol. 11, no. 2, pp. 96–102, 2004.

[9] X. Guo, J. Baroth, D. Dias, and A. Simon, "An analytical model for the monitoring of pore water pressure inside embankment dams," *Eng. Struct.*, vol. 160, pp. 356–365, 2018. https://doi.org/10.1016/j.engstruct.2018.01.054

[10] K. Adalier and M. K. Sharp, "Embankment dam on liquefiable foundation—Dynamic behavior and densification remediation," *J. Geotech. Geoenviron.*, vol. 130, no. 11, pp. 1214–1224, 2004.

[11] W. Ross Boulanger, J. Montgomery, and K. Ziotopoulou, "Nonlinear deformation analyses of liquefaction effects on embankment dams," in *Perspectives on Earthquake Geotechnical Engineering: In Honour of Prof. Kenji Ishihara*, 2015, pp. 247–283. https://doi.org/10.1007/978-3-319-10786-8_10

[12] J. Montgomery, "Issues in nonlinear deformation analyses of embankment dams affected by liquefaction," 2015. https://www.proquest.com/openview/8fd1700754971234d12bf0f3f7c13d4f/1?cbl=18750&pq-origsite=gscholar&login=trues://www.proquest.com/openview/8fd1700754971234d12bf0f3f7c13d4f/1?cbl=18750&pq-origsite=gscholar&login=true

[13] S. M. Seyedi-Viand and E. Ece Eseller-Bayat, "Partial saturation as a liquefaction countermeasure: A review," *Geotech. Geol. Eng.*, vol. 40, no. 2, pp. 499–530, 2021. https://doi.org/10.1007/s10706-021-01926-5

[14] S. M. Seyedi-Viand and E. Ece Eseller-Bayat, "An alternative empirical function to predict air–water mixture bulk modulus for numerical modeling of liquefaction behavior of induced partially saturated sands," *B. Earthq. Eng.*, vol. 19, no. 5, pp. 1987–2011, 2021. https://doi.org/10.1007/s10518-021-01058-4

[15] S. M. S. Viand and E. E. Eseller-Bayat, "Numerical modelling of liquefaction tests of partially saturated sands in CSSLB," in *Advances in Laboratory Testing and Modelling of Soils and Shales (ATMSS)*, 2017, pp. 501–508. https://doi.org/10.1007/978-3-319-52773-4_60

[16] A. Soroush and P. Tabatabaie Shourijeh, "Measures to prevent internal erosion in embankment dams," in *Sustainable and Safe Dams Around the World*, 2019, pp. 854–867. https://doi.org/10.1201/9780429319778-74

[17] A. Torabi Haghighi, A. Tuomela, and A. A. Hekmatzadeh, "Assessing the efficiency of seepage control measures in earthfill dams," *Geotech. Geol. Eng.*, vol. 38, no. 5, pp. 5667–5680, 2020. https://doi.org/10.1007/s10706-020-01371-w

[18] M. A. M. AL-Dulaimi and M. Seyedi, "Numerical analysis of geogrids and recycled concrete aggregate for stabilizing road embankments," *Annales de Chimie - Science des Matériaux*, vol. 47, no. 4, pp. 219–223, 2023. https://doi.org/10.18280/acsm.470404

[19] B. V. Plaxis, *PLAXIS material models manual*, 2018. https://comhttps://communities.bentley.com/cfs-file/__key/communityserver-wikis-components-files/00-00-00-05-58/0118.PLAXIS3DCE_2D00_V20.02_2D00_3_2D00_Material_2D00_Models.pdfmunities.bentley.com/cfs-file/__key/communityserver-wikis-components-files/00-00-00-05-58/0118.PLAXIS3DCE_2D00_V20.02_2D00_3_2D00_Material_2D00_Models.pdf

[20] T. Schanz, P. A. Vermeer, and P. G. Bonnier, "The hardening soil model: Formulation and verification," in *Beyond 2000 in Computational Geotechnics*, 1999, pp. 281–296. https://doi.org/10.1201/9781315138206

[21] A. Petalas and V. Galavi, "Plaxis liquefaction model UBC3D-PLM," 2013.

[22] C. S. Undayani, W. Partono, and S. P. Retno Wardani, "Displacement analysis of dam based on material parameters using numerical simulation and monitoring instrumentation," in *MATEC Web of Conferences*, vol. 258, 2019. https://doi.org/10.1051/matecconf/201925805013

[23] S. R. Tafti, A. Shafiee, and M. M. Rajabi, "The influence of clay core composition on the permanent displacement of embankment dams," in *Proceedings of the 14th World Conference on Earthquake Engineering*, 2008, pp. 1–8. httphttps://iitk.ac.in/nicee/wcee/article/14_04-01-0059.PDFs://iitk.ac.in/nicee/wcee/article/14_04-01-0059.PDF

Nomenclature

DOF	Degree of freedom
HS small	Hardening soil model with small-strain stiffness
PLM	PLAXIS Liquefaction Model
SPT	Standard Penetration Test
D_r	Relative density
γ_{sat}	Saturated unit weight
${E_{50}}^{ref}$	Secant stiffness in standard drained triaxial test
${E_{oed}}^{ref}$	Tangent stiffness for primary oedometer loading
${E_{ur}}^{ref}$	Unloading/reloading stiffness from drained triaxial test
${G_0}^{ref}$	Reference shear modulus at very small strains $\left(\varepsilon < 10^{-6}\right)$
m	Power for stress-level dependency of stiffness
$\gamma_{0.7}$	Threshold shear strain at which $G_s = 0.722G_0$
C'_{ref}	Cohesion of the soil
R_f	Failure ratio
$(N_1)_{60}$	Corrected SPT value
φ_{cv}	Constant volume friction angle
K_G^{*e}	Elastic shear modulus factor
K_B^{*e}	Elastic bulk modulus factor
K_G^{*p}	Plastic shear modulus factor
m_e	Rate of stress-dependency of elastic bulk modulus
n_e	Rate of stress-dependency of elastic shear modulus
n_p	Rate of stress-dependency of plastic shear modulus
p_{ref}	Reference pressure

Greek symbols

φ'	Soil friction angle
v	Poisson ratio